H2020-FETFLAG-2018-2021

macQsimal

Miniature **A**tomic vapor-**C**ell **Q**uantum devices for **S**ens**I**ng and **M**etrology **A**pp**L**ications

Deliverable 4.6

High-density OPM demonstrator and benchmarking report

WP4 – Miniature optically-pumped magnetometers

Authors: Lauri Parkkonen (AALTO)

Lead participant: AALTO

Delivery date: 29.07.2022

Dissemination level: Public

Type: R (Document, Report)

This work has received funding from the European Union's Horizon 2020 research and innovation programme under grant agreement No. 820393.

Revision History

Author Name, Partner short name	**Description**	**Date**
Lauri Parkkonen (AALTO)	Initial draft	14.07.2022
Morgan Mitchell (ICFO)	Review and small fixes	26.07.2022
Kostas Mouloudakis (ICFO)	Lab setup spectra	26.07.2022
Michael Tayler (ICFO)	More details of the lab set-up	27.07.2022
Rasmus Zetter (MEGIN)	Review and additions to evaluation	27.07.2022
Petteri Laine (MEGIN)	Review and approval	28.07.2022
Lauri Parkkonen (AALTO)	Incorporation of the comments	28.07.2022
Andreia Cruz (accelCH)	Formal checks and formatting	29.07.2022

Abbreviations

AEF	Auditory evoked field
EC	European Commission
EU	European Union
FAQ	Frequently Asked Questions
FPGA	Field-programmable gate array
H2020	Horizon 2020
LTCC	Low-temperature co-fired ceramic
MEG	Magnetoencephalography
MEMS	Microelectromechanical system
OPM	Optically pumped magnetometer
PCB	Printed circuit board
QT	Quantum Technologies
SERF	Spin exchange relaxation-free
SQC	SQUID controller card
SQUID	Superconducting quantum interference device
TRL	Technology readiness level
VCSEL	Vertical-cavity surface-emitting laser
WP	Work Package

Partner short names

ACCEL	accelopment AG, CH
AALTO	Aalto Korkeakoulusaatio SR, FI
CSEM	CSEM SA – Centre Suisse d'Électronique et de Microtechnique, CH
ICFO	Fundació Institut De Ciéncies Fotòniques, ES
MEGIN	MEGIN OY (formerly Elekta Oy), FI
VTT	Teknologian Tutkimuskeskus VTT Oy, FI

Contents

Executive Summary

This Deliverable documents how the high-density OPM developed in WP4 of the macQsimal project performs and specifically how it could be used in magnetoencephalographic (MEG) measurements, i.e., detecting the extremely weak magnetic fields due to electric activity in the human brain.

The deliverable is linked to task T4.1.5. and the contents are provided mainly by AALTO, ICFO and MEGIN.

Need for the Deliverable

The Deliverable describes the state to which the macQsimal project proceeded in terms of the MEG application of the high-density OPM sensor.

Objectives of the Deliverable

The Deliverable aims to document the following items:

- the achieved high-density OPM performance,
- the determined requirements for successful MEG measurements, and
- comparison of the above.

Outcomes

The OPM sensor developed in the macQsimal project showed clearly sufficient performance for MEG measurements, with potential to exceed the state of the art in compact SERF OPM sensors suitable for MEG; however, the integration of the sensor could not be completed within the time frame of the project and therefore the testing had to be done in two separate stages. First, the performance of the macQsimal sensor was evaluated in an optics bench at ICFO, and second, commercially available OPM sensors were applied in a MEG measurement by AALTO in a typical hospital setting. The comparison of these experiments demonstrated that the macQsimal sensor would be suitable for MEG provided the sensor integration could be completed.

Next steps

Sensor integration shall be continued to yield the compact, high-performance OPM sensor suitable for MEG; the project was not sufficiently long to reach this goal. Fortunately, there are no foreseeable major technical obstacles to this end.

1 High-density OPM sensor

1.1 Working principle

The higher-TRL high-density OPM sensor developed in the macQsimal project is a SERF magnetometer employing a single laser at 795 nm, ^{87}Rb MEMS dual-chamber vapour cell with buffer gas, a pair of photodetectors and field modulation and compensation coils around the cell. The basic principle (without the field coils) is illustrated in Fig. 1. The vapour cell was developed in WP3 of macQsimal; see the corresponding deliverables for further details.

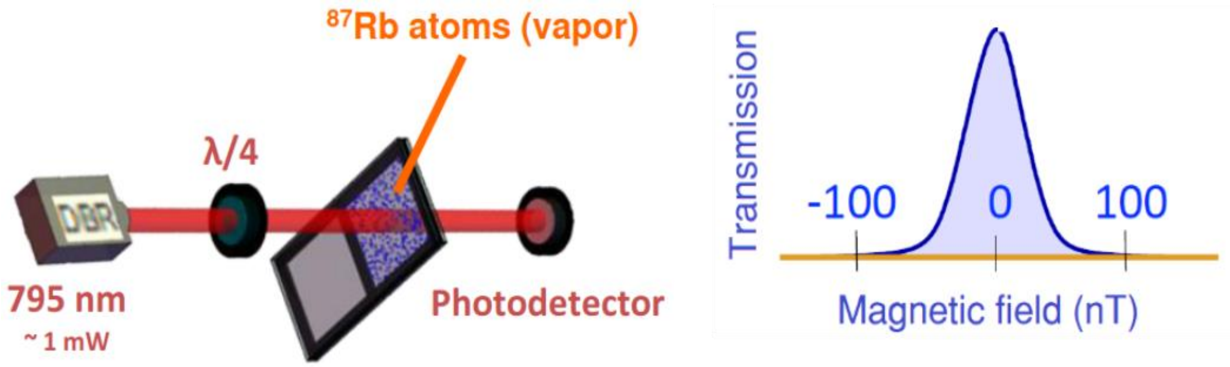

Figure 1: A single-laser SERF OPM working principle. The transmission of the laser beam through the Rubidium vapour depends on the applied magnetic field and is measured by a photodetector.

1.2 Field coils

In order to provide maximally homogeneous field throughout the vapour cell and to minimize cross-talk between neighbouring sensors, the macQsimal OPM employs self-shielding biplanar coils, recently published by the consortium members (Tayler et al., 2022). The optimal wiring patterns were determined using stream-function formalism as implemented in the 'bfieldtools' open-source software package (Mäkinen et al., 2020; Zetter et al., 2020) that we have developed in the context of the macQsimal project. The coils were then implemented as two multi-layer printed circuit boards (PCB) as shown in Fig. 2.

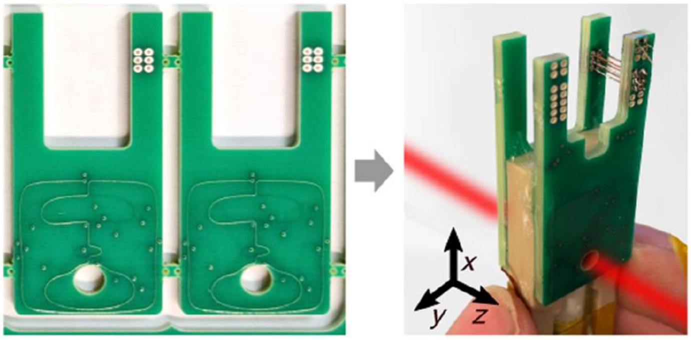

Figure 2: Self-shielding biplanar coils. The vapour cell of the OPM sensor is surrounded by two multilayer PCBs that contain the coil wiring patterns. These coils can produce homogeneous fields in the three orthogonal directions within the vapour cell while minimizing the stray field around the sensor housing. Adapted from (Tayler et al., 2022).

1.3 Sensor head

The optics and coils are assembled into a compact housing (20 x 20 x 54 mm^3) that can readily be applied on the scalp of the study subject for MEG measurements. A CAD model is shown in Figure 3.

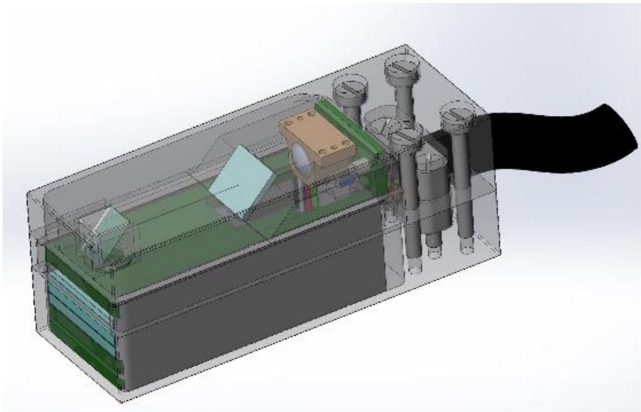

Figure 3: High-density OPM sensor head.

1.4 Electronics and software

The electronics in the sensor head include the photodetectors and their low-noise pre-amplifiers, VCSEL, cell and VCSEL heaters and thermistors to measure the VCSEL and cell temperatures. The sensor-head electronics are read out and controlled by an adapted version of MEGIN's SQUID controller card (SQC) that houses high-performance A/D and D/A converters for 12 channels, an FPGA, and a Linux-based microcontroller with an Ethernet interface. For the macQsimal OPM sensor, the FPGA was reprogrammed to support OPM-specific functions such as VCSEL control, cell heating control, field modulation and photodetector signal demodulation; a block diagram of the FPGA functions is shown in Fig. 4b.

To electrically interface the sensor head and SQC, a custom electronics board (see Fig. 4a) was developed in macQsimal. This board provides matching of signal levels and impedances and drives the heaters and the VCSEL.

To operate the whole sensor system and to acquire data, the MEGIN data acquisition system was adapted for OPM use. A new piece of software (“serfer”) with a graphical user interface was written to enable examining and adjusting OPM operating parameters in an easy manner; see Fig. 4c.

For the tests at ICFO, a simple low-power electronics systems provided the highest magnetic sensitivity in the controlled test environment, at expense of other performance factors, e.g. sensor dynamic range. Magnetic noise spectra presented in this report for the lab-bench OPM setup were acquired in open-loop (no field feedback) sensor mode using a commercial 24-bit audio codec chip (CS4272) interfaced with a microcontroller (ARM Cortex M7).

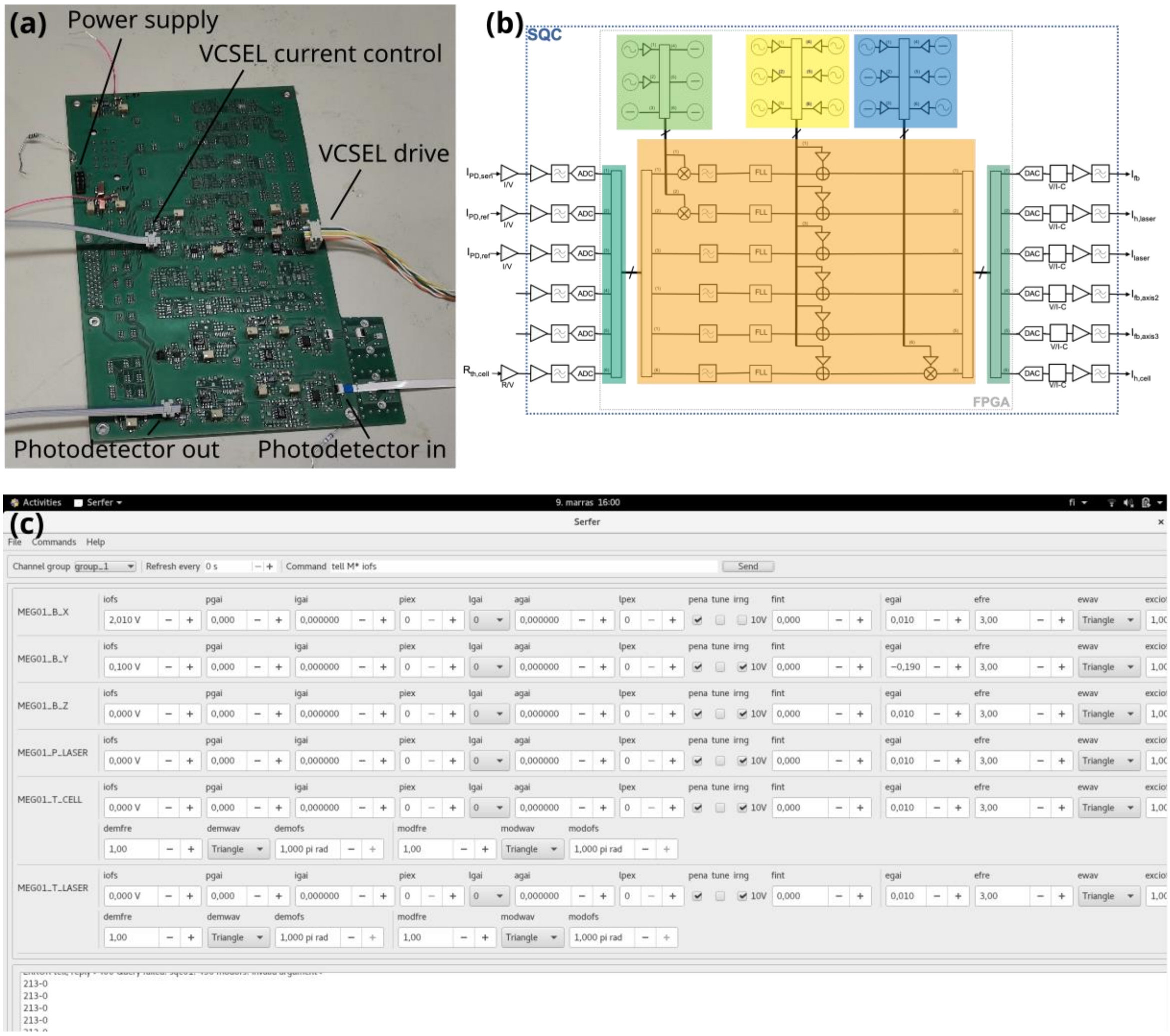

Figure 4: Electronics and software. (a) The interface electronics board between the OPM sensor head and the SQC board. (b) Block diagram of the functions of the FPGA on the SQC board. (c) Screen shot of the "serfer" OPM parameter control software.

2 Measurements in a laboratory set-up

A non-packaged version of the sensor head was tested in a table-top magnetic shield (MS-1LF; Twinleaf LLC, NJ, USA) on an optics bench at ICFO. The electronics and software described in Section **Error! Reference source not found.** was employed to drive and read out the sensor.

2.1 Sensitivity

The measurement demonstrated sensitivity of 10–15 fT/Hz$^{-1/2}$ in the white-noise region; see Figure 5. The 1/f-noise corner frequency is at few Hertz; however, we cannot exclude the contribution of ambient noise sources (external to the shield) and thus the OPM sensor may perform better in this respect.

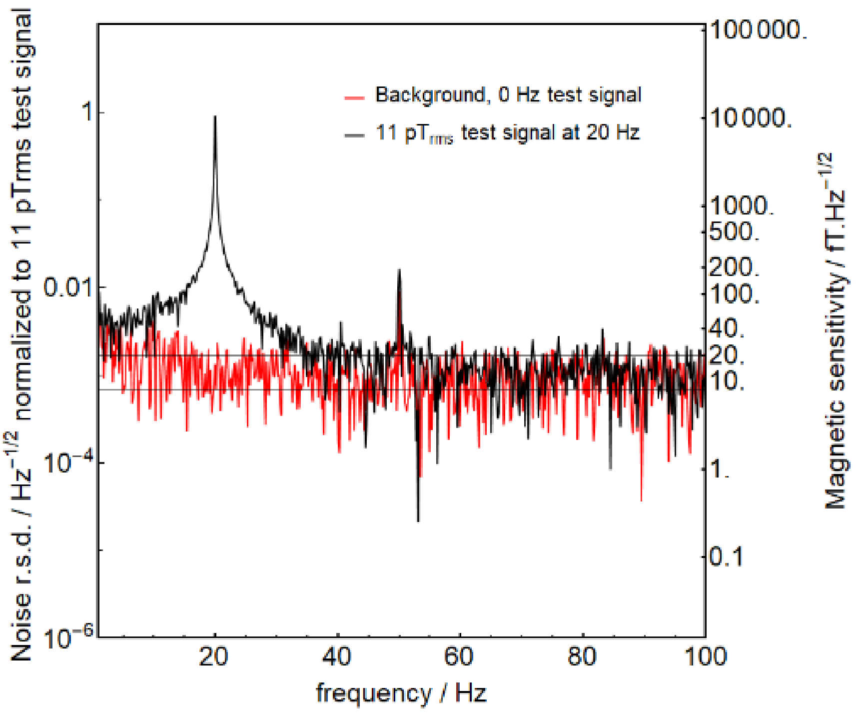

Figure 5: High-density OPM sensitivity in a table-top magnetic shield.

2.2 Frequency response

The spectrum in Fig. 5 shows flat frequency response at least in the range 1–100 Hz.

2.3 Cross-talk

We conducted measurements of the stray-field profiles produced by the field coils in a magnetic shield using a commercial OPM sensor (QZFM Gen 2; QuSpin Inc., CO, USA). Figure 6 shows the results of these measurements; the estimated and measured values are in a good agreement, confirming that the self-shielding function works as intended. More details are available in our publication (Tayler et al., 2022).

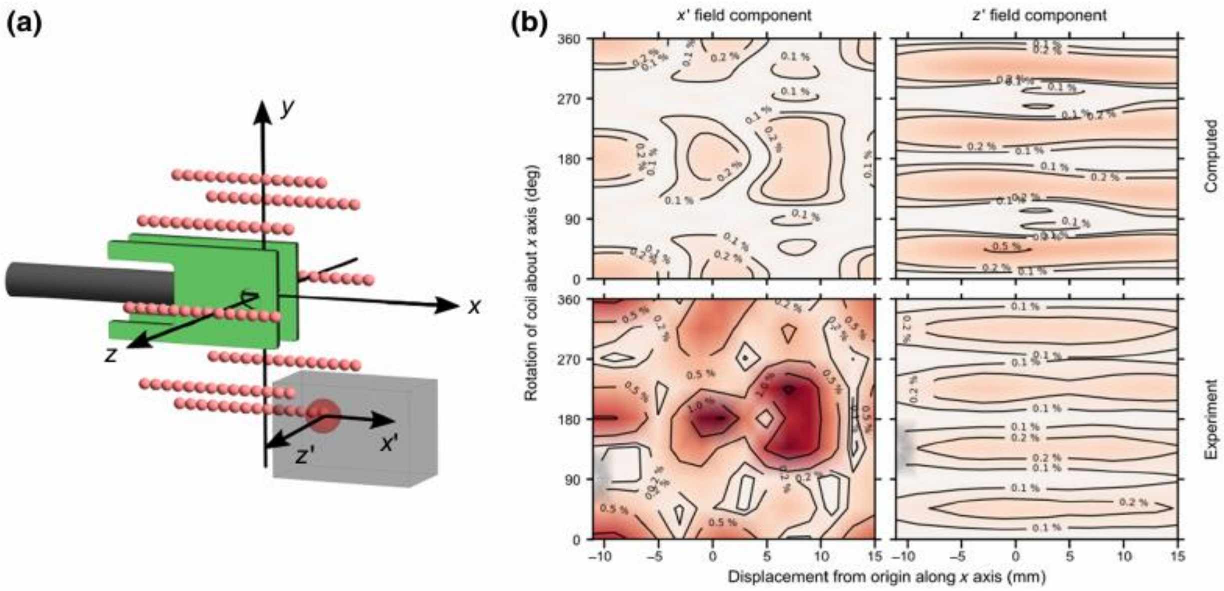

Figure 6: Stray-field measurement and maps of the biplanar coil structure. (a) The measurement set-up; the pink spheres indicate the field sampling locations. (b) The estimated and measured field magnitudes produced by the 'X' coil.

2.4 Surface temperature

Since the final sensor housing could not yet be used in the measurements, we did not record the surface temperature as of now.

3 Measurements in a magnetically shielded room

To assess if the attained OPM sensor performance is sufficient for clinical MEG investigations, we examined the magnetic environment within a magnetically shielded room installed in a hospital (BioMag laboratory at Helsinki University Central Hospital). We also conducted OPM MEG measurements in that shielded room using commercially available OPM sensors.

3.1 Magnetic environment

The magnetically shielded room (ETS-Lindgren Oy, Eura, Finland) is installed in the basement of a large hospital. The room has three aluminium and three mu-metal layers. The inner dimensions are about 2.5 x 3.5 x 2.3 m^3 (width, length, height). No degaussing of the room was performed prior to these measurements.

Measurements with a flux-gate sensor indicated a remnant DC field of about 30 nT at the centre of the room.

3.2 OPM measurement set-up

Altogether 15 OPM sensors (QZFM Gen 1 and 2; QuSpin Inc., CO, USA) were employed in the measurement. According to the vendor specification, the sensitivity of these sensors is < 15 $fT/Hz^{-1/2}$.

The OPM sensors were inserted in pre-determined slots in a custom-made helmet that follows the geometry of the sensor helmet of the MEGIN SQUID-based MEG system. The helmet was attached to a non-magnetic bed.

A modified version of MEGIN SQC boards and data acquisition system were utilized to read and condition the analogue signals from QuSpin OPM electronics. Further details of the system are available in our publication (Iivanainen et al., 2019). The OPM signals were low-pass-filtered to 330 Hz and sampled at 1 kHz.

To null the remnant DC field inside the shielded room, we employed custom-made large biplanar coils, designed with “bfieldtools” (Mäkinen et al., 2020; Zetter et al., 2020) and drove them with an adjustable low-noise DC current source (by Zetter at MEGIN) such that the DC field as measured by the OPMs was minimal (less than 5 nT); see Fig. 7a.

The OPM sensor array was installed roughly at the centre of the room at the height of 90 cm (helmet centre) above the inner floor. Figure 7a shows the measurement set-up inside the shielded room. The OPM sensors were placed above the left temporal (10 sensors) and occipital (5 sensors) areas; see Fig. 7b.

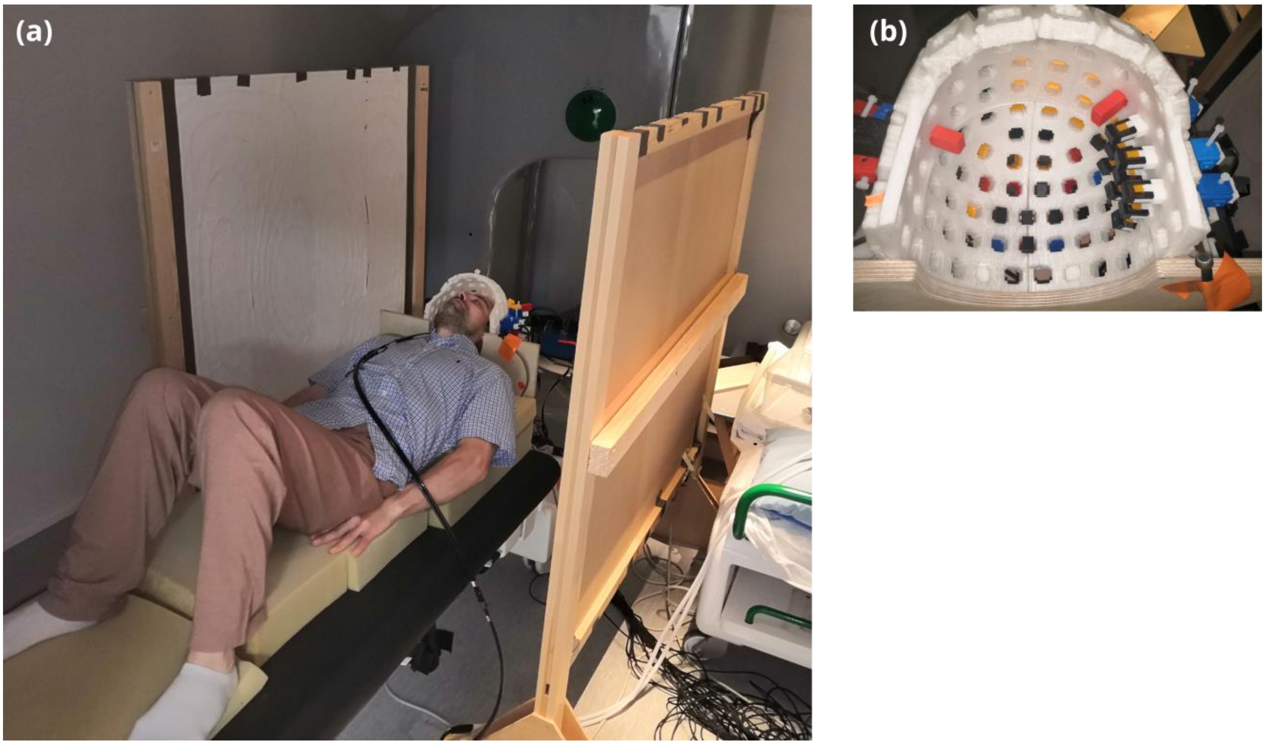

Figure 7: OPM MEG measurement. (a) The field-nulling biplanar coils are on the sides of the subject whose head is in the OPM sensor helmet. (b) The sensor helmet is populated with OPMs (black) and dummy blocks (red) to help keep the head immobile within the helmet.

3.3 Measurement protocol

We recorded resting-state brain activity while the subject was opening/closing his eyes every 30 s, instructed by the operator via an intercom. A total of 3 min (6 x 30 s) was recorded.

We also recorded auditory evoked fields (AEF); the subject was presented with brief 1-kHz tone pips to the right ear via a plastic tube from a loudspeaker outside of the magnetically shielded room. This tone pip was repeated every 2 s, and about 200 such trials were recorded. The AEF results are not presented in this report.

3.4 Results

Figure 8 shows the amplitude spectra (Welch method, Hamming window, 4096-point FFT) of OPM data acquired without a subject and with the subject resting. Brain signals dominate the spectra up to about 40 Hz, after which the sensor noise appears equal or larger than brain signals. The prominent peaks at 8–10 Hz and 15–18 Hz correspond to the alpha and beta rhythms of the brain, respectively.

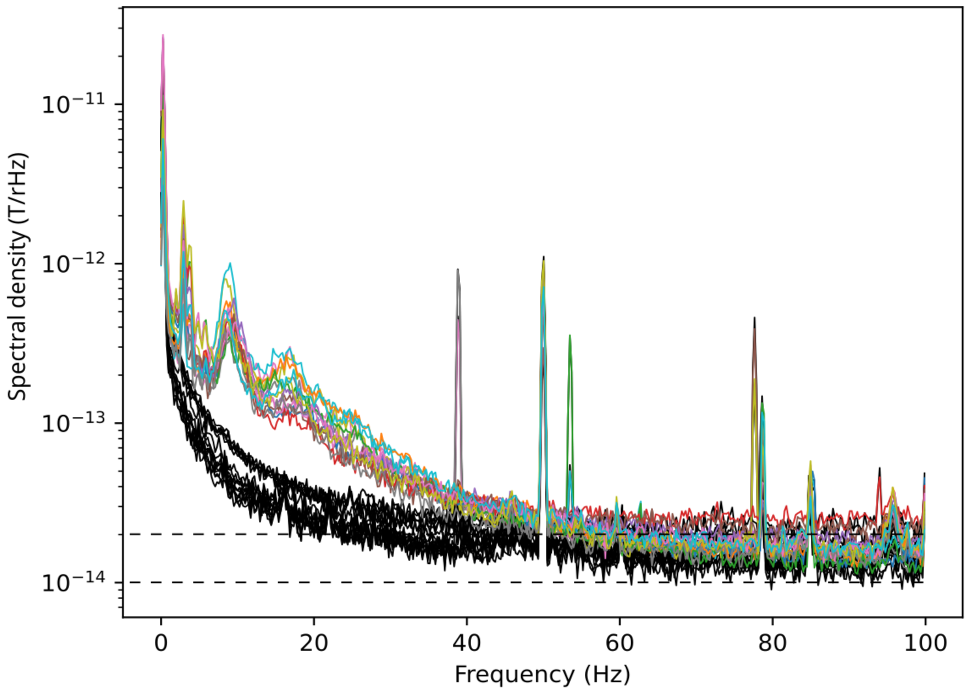

Figure 8: Spectra of the 15 OPM signals recorded in the absence of a subject (black lines) and with the subject resting (coloured lines). The 10- and 20-fT/Hz$^{-1/2}$ levels are marked (dashed lines).

4 Evaluation of the results

This section presents a comparison of the laboratory and shielded-room measurements.

4.1 Sensitivity and frequency response

The noise spectra from the macQsimal sensor (same data as in Fig. 5 red trace) and from the commercially available OPM sensors (same data as in Fig. 8 but spectra averaged across sensors) are shown overlaid in Fig. 9. Since the set-up with commercial sensors (see Section 3.2) comprised not one but 15 sensors, their spectra were averaged for easier comparison to the macQsimal sensor. This averaging also reduced the variance of the spectral estimate as is apparent in the figure.

Even though the two measurements were performed in different kind of magnetic shields (table-top shield in a laboratory vs. magnetically shielded room in a hospital) and different electronics were employed, we can state – based on these results – that the sensitivity of the macQsimal OPM sensor is comparable if not better than that of the reference commercial offering and that it appears sufficient for

MEG particularly at frequencies below 60 Hz or so; above these frequencies MEG signals produced by on-going brain activity do not seem to exceed the sensor noise level.

The frequency response of the macQsimal sensor appears on par with the commercial offering, i.e., from DC up to 100 or 150 Hz, which is wide enough for most MEG use since the bulk of the brain signals occur at frequencies below 100 Hz.

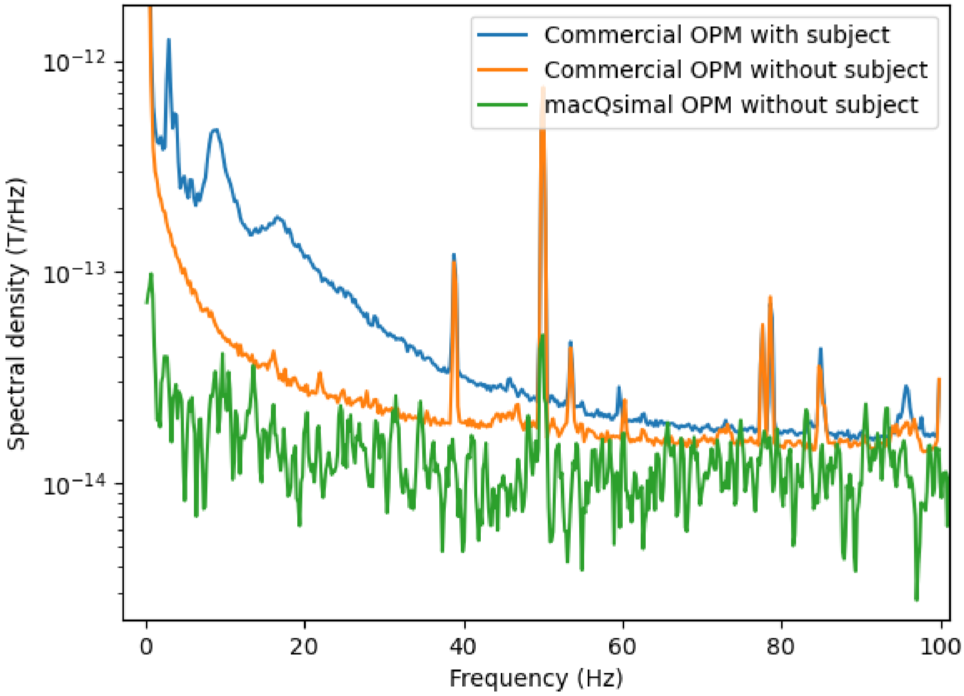

Figure 9: Comparison of the noise spectra (sensitivities) of the macQsimal sensor (green; one sensor) and the commercially available sensors (orange and blue; average of the 15 sensors). The commercial sensors were utilized in the same arrangement and same magnetically shielded room both in the absence (orange) and presence (blue) of a study subject.

4.2 Other performance characteristics

Since the macQsimal project will end before the fully assembled OPM sensor head is available for measurements, we could not measure characteristics such as dynamic range, cross-talk and surface temperature.

Yet, based on the laboratory tests described earlier in this report (see Section 2.3) we foresee that cross-talk would become significantly lower than the state of the art at the moment. Similarly, the utilization of negative feedback (see Section 1.4) should expand the dynamic range and improve linearity beyond current offerings.

The LTCC-based vacuum packaging of the vapour cell should result in a significantly lower surface temperature than what has been achieved before. This would be a very important advance for the applicability of OPM MEG in a clinical setting.

5 Bibliography

Iivanainen, J., Zetter, R., Grön, M., Hakkarainen, K., Parkkonen, L., 2019. On-scalp MEG system utilizing an actively shielded array of optically-pumped magnetometers. NeuroImage 194, 244–258. https://doi.org/10.1016/j.neuroimage.2019.03.022

Mäkinen, A.J., Zetter, R., Iivanainen, J., Zevenhoven, K.C.J., Parkkonen, L., Ilmoniemi, R.J., 2020. Magnetic-field modeling with surface currents. Part I. Physical and computational principles of bfieldtools. J. Appl. Phys. 128, 063906. https://doi.org/10.1063/5.0016090

Tayler, M.C.D., Mouloudakis, K., Zetter, R., Hunter, D., Lucivero, V.G., Bodenstedt, S., Parkkonen, L., Mitchell, M.W., 2022. Miniature Biplanar Coils for Alkali-Metal-Vapor Magnetometry. Phys. Rev. Appl. 18, 014036. https://doi.org/10.1103/PhysRevApplied.18.014036

Zetter, R., J. Mäkinen, A., Iivanainen, J., Zevenhoven, K.C.J., Ilmoniemi, R.J., Parkkonen, L., 2020. Magnetic field modeling with surface currents. Part II. Implementation and usage of bfieldtools. J. Appl. Phys. 128, 063905. https://doi.org/10.1063/5.0016087